

# Chase-and-run dynamics in cell motility and the molecular rupture of interacting active elastic dimers

David Mayett,<sup>1</sup> Nicholas Bitten,<sup>2</sup> Moumita Das,<sup>2</sup> and J. M. Schwarz<sup>1</sup>

<sup>1</sup>*Department of Physics, Syracuse University, Syracuse, NY 13244, USA*

<sup>2</sup>*School of Physics and Astronomy, Rochester Institute of Technology, Rochester, NY 14623, USA*

(Dated: March 10, 2022)

Cell migration in morphogenesis and cancer metastasis typically involves interplay between different cell types. We construct and study a minimal, one-dimensional model comprised of two different motile cells with each cell represented as an active elastic dimer. The interaction between the two cells via cadherins is modeled as a spring that can rupture beyond a threshold force as it undergoes dynamic loading via the attached motile cells. We obtain a phase diagram consisting of chase-and-run dynamics and clumping dynamics as a function of the stiffness of the interaction spring and the threshold force. We also find that while feedback between cadherins and cell-substrate interaction via integrins accentuates the chase-run behavior, feedback is not necessary for it.

During embryonic development as well as in cancer metastasis, cells often undergo migration in groups [1]. Such groups are typically composed of cells of different types interacting with each other giving rise to nontrivial migration modes. For example, co-cultures of stromal fibroblasts and carcinoma cells on top of an extracellular matrix (ECM) reveal that the carcinoma cells move within tracks in the ECM made by the fibroblasts [2]. Another example of a nontrivial migration mode occurs when neural crest (NC) cells and placodal (PL) cells are cultured next to each other on a polyacrylamide substrate. The NC cells start chasing the PL cells via chemotaxis, while the PL cells run away from the NC cells when contacted by them [3]. NC cells are highly multipotent cells that migrate extensively during embryogenesis, and eventually differentiate to give rise to multiple cell types including some nerve and glial cells, fibroblasts, and smooth muscle cells [4]. Placodal cells (PL), on the other hand, are embryonic cells that remain more localized [3]. They play a critical role in development of the cranial sensory system in vertebrates[5].

While there are a number of models of single cell migration or few cell migration of the same cell type on surfaces [6, 7, 9–14, 20], the rules governing the interplay between different cell types from a cell migration standpoint remain largely unknown. Inspired by the NC/PL cell experiment [3], we consider a minimal, one-dimensional model of two different, but interacting, cells. Each cell is modeled as an active elastic dimer with focal adhesions acting as catch bonds at the leading edge of a crawling cell and slip bonds at its rear [15]. The mechanosensitive activity, which is incorporated as a changing equilibrium spring length depending on the loading state of myosin, combined with the catch/slip bond asymmetry generates motion even in the absence of broad lamellipodia typically observed in cells crawling along two-dimensional surfaces [7]. By invoking a minimal set of assumptions for the interaction between the two cells in our one-dimensional model, we can predict, in principle, all possible migration outcomes and, therefore, begin to classify the rules of interplay between two motile

cells. More specifically, we can observe nontrivial migration modes such as the chase-and run phenomenon and ultimately distinguish between various mechanisms for contact-inhibition-locomotion (CIL)—motion in which two cells move towards each other, collide, and then move away from each other [3, 16, 17]. Both behaviors are fundamentally one-dimensional and can therefore be captured with our one-dimensional model capturing mesenchymal migration along a taut ECM fiber, for example.

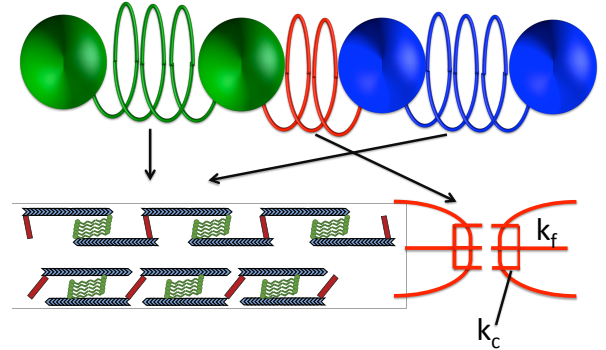


FIG. 1. (Color Online) Schematic representation of two cells (blue and green) with the red interaction spring containing  $N$  cadherin molecules in parallel, each with spring stiffness  $k_c$  and a filopod with spring stiffness  $k_f$ . Each blue and green spring represents the prominent stress fibers along the length of the cell and, therefore, is active with both the extended mode (top) and contracted mode (bottom). The blue filaments represent actin filaments, red rectangles, alpha-actinin, and the green shapes, myosin minifilaments.

*Model:* Cells moving along ECM fibers or patterned microchannels extend themselves along the fiber/channel and move even in the absence of lamellipodia [18–22]. Pronounced stress fibers are a characteristic feature of this migration mode called mesenchymal migration [18]. Stress fibers primarily consist of actin filaments, myosin, and a passive cross-linker alpha-actinin [23]. Structurally, they can be thought of as made of parallel arrangements of acto-myosin units in series, where each actomyosin unit may be considered as two actin filaments

connected by a myosin mini-filament, and the crosslinker alpha-actinin at each end (Fig. 1). We have previously developed a model to describe a single cell in this migration mode [15] which serves as the foundation for our investigation of two co-migrating interacting cells.

The main ingredients of the single cell model, which has been studied in detail in [15] and reviewed in the SI, are as follows:

(1) The migrating cell is modeled as two beads connected by an active spring. The spring represents the stress fiber and the beads denote the location of focal adhesions at positions, say,  $x_1$  and  $x_2$ , which enable the stress fibers connect to the ECM fiber.

(2) The active spring has two different equilibrium lengths,  $x_{eq1}$  and  $x_{eq1} - x_{eq2}$ , corresponding to the nearly unloaded and loaded states of myosin. The former is determined mainly by passive alpha-actinin driven extension and the latter by active myosin driven contraction. The equilibrium spring length,  $x_{eq}$ , can then be written as  $x_{eq} = x_{eq1} - x_{eq2}\Theta(x_1 - x_2 - l)$  where  $\Theta(x_1 - x_2 - l)$  is the Heaviside step function. The transition between the two modes is determined by the extension of the spring: the larger the extension, the more the tensile load on myosin thereby inducing contractility of myosin given its catch bond nature [24].

(3) There exists hysteresis in the equilibrium spring length with  $l = l^\uparrow$  as the active spring extends and  $l = l^\downarrow \neq l^\uparrow$  as it compresses due to increasing overlap between actin filaments allowing for more passive crosslinking by alpha-actinin, potential conformational changes in the alpha-actinin, and internal frictional losses.

(4) Integrins, one of the principal proteins in focal adhesions adhering the cell to the fiber [25], can act as catch bonds under repeated loading [26]. They are more likely to act as catch bonds at the leading edge of a crawling cell due to the more dynamic environment for the maturation of focal adhesions, while at the rear they act as typical slip bonds where focal adhesions are merely being disassembled. So, at the front of the cell, the initiation of focal adhesions call for a “small” friction coefficient, but once the focal adhesions form and develop, the friction increases. This “catching” mechanism of cell-track adhesion allows the cell’s front to expand and explore new territory and after having done that, then allows for the cell’s rear to retract with the cell front not losing grip on the new territory it just explored. So we define the friction coefficient at the leading edge to be  $\gamma_1 = \gamma_{11} + \gamma_{12}\Theta(x_1 - x_2 - l^{\uparrow(\downarrow)})$  with  $\gamma_{11}, \gamma_{12} > 0$  and  $\gamma_{11} < \gamma_{12}$ . Because the integrins track myosin activity, the hysteresis exhibited by myosin is also exhibited in the friction. Finally,  $\gamma_2$ , the friction coefficient for the now “rear” bead, is assumed to be constant with the integrins acting as ordinary slip bonds.

(5) The combination of activity that depends on the strain in the stress fiber and the asymmetry of the focal adhesions at the leading and rear edges leads to directed cell motion in the direction of larger friction [27].

To address the interaction between two motile cells

in one-dimension, each cell is described by above single cell model. To be concrete, the beads are described by their positions  $x_i(t)$ , with  $i \in [1, 4]$ , where  $i = 1$  denotes the rightmost bead and  $i = 4$  the leftmost. The focal adhesions associated with the  $i^{th}$  bead are denoted by  $\gamma_i$ . For the cell on the right,  $\gamma_1 = \gamma_2$ . This cell is stationary given the symmetry in the friction, provided no outside forces act on it. This is our model PLL (placode-like) cell. As for our neural crest-like (NCL) cell (cell on the left), the action of chemotaxis is implicitly described by the breaking of the symmetry between the rear and front bead focal adhesion of the left cell to generate directed motion. Thus, for the cell on the left we have  $\gamma_3 = \gamma_{33} + \gamma_{34}\Theta(x_3 - x_4 - l^{\uparrow(\downarrow)})$  and  $\gamma_4$  is a constant. Both cells have changing equilibrium spring lengths denoted by  $x_{eq} = x_{eq1} - x_{eq2}\Theta(x_1 - x_2 - l^{\uparrow(\downarrow)})$  (for the PLL cell) to incorporate myosin driven contractility and  $\alpha$ -actinin driven extensibility as described in [15].

The cell-cell interactions are mediated by cadherin molecules. These molecules localize at the ends of filopodia (small actin-bundle-based protrusions) demonstrating that cadherins also interact with the actin cytoskeleton [28]. The number of cadherin molecules at the tips of filopodia and other actin-based protrusions range from hundreds to thousands. We assume that cadherin molecules, each modeled as a linear spring with spring constant  $k_c$ , bind in parallel and are then bound to a filopod also modeled as another linear spring with spring constant  $k_f$ . See Fig. 1. When the two cells come in close enough proximity, an interaction spring forms between them. This proximity is denoted by  $l_a$ . Because the two cells have their own inherent dynamics, they can in principle pull on the cadherin bonds and rupture them [29]. For simplicity, we assume the interaction spring can rupture when  $k_f(x_2 - x_3 - l_{eq}) > N_0 f_c$ , where  $f_c$  is the critical force threshold that will rupture an individual cadherin bound for  $k_f \approx k_c$  with  $k_f = k$  for notational ease. Rupture can only occur when the two beads at either end of the interaction spring are moving away from each other.

Putting together the different components of the model, the four coupled equations of motion of the beads are as follows:

$$\begin{aligned} \gamma_1(x_1, x_2, l^\uparrow, l^\downarrow)\dot{x}_1(t) &= -k_1 \left[ x_1 - x_2 - x_{eq}(x_1, x_2, l^\uparrow, l^\downarrow) \right] \\ &\quad + \sqrt{A_1}\zeta_1(t) \\ \gamma_2(x_1, x_2, l^\uparrow, l^\downarrow)\dot{x}_2(t) &= k_1 \left[ x_1 - x_2 - x_{eq}(x_1, x_2, l^\uparrow, l^\downarrow) \right] \\ &\quad - k_c[x_2 - x_3 - l_{eq}] + \sqrt{A_2}\zeta_2(t) \\ \gamma_3(x_3, x_4, l^\uparrow, l^\downarrow)\dot{x}_3(t) &= -k_2 \left[ x_3 - x_4 - x_{eq}(x_3, x_4, l^\uparrow, l^\downarrow) \right] \\ &\quad + k_c[x_2 - x_3 - l_{eq}] + \sqrt{A_3}\zeta_3(t) \\ \gamma_4(x_3, x_4, l^\uparrow, l^\downarrow)\dot{x}_4(t) &= k_2 \left[ x_3 - x_4 - x_{eq}(x_3, x_4, l^\uparrow, l^\downarrow) \right] \\ &\quad + \sqrt{A_4}\zeta_4(t). \end{aligned}$$

For completeness, we have included fluctuations denoted by  $\sqrt{A_i}\zeta_i(t)$ , where  $\zeta_i(t)$  is a Gaussian random variable with  $\langle \zeta_i(t) \rangle = 0$  and  $\langle \zeta_i(t)\zeta_j(t') \rangle = \delta_{ij}\delta(t-t')$ . These

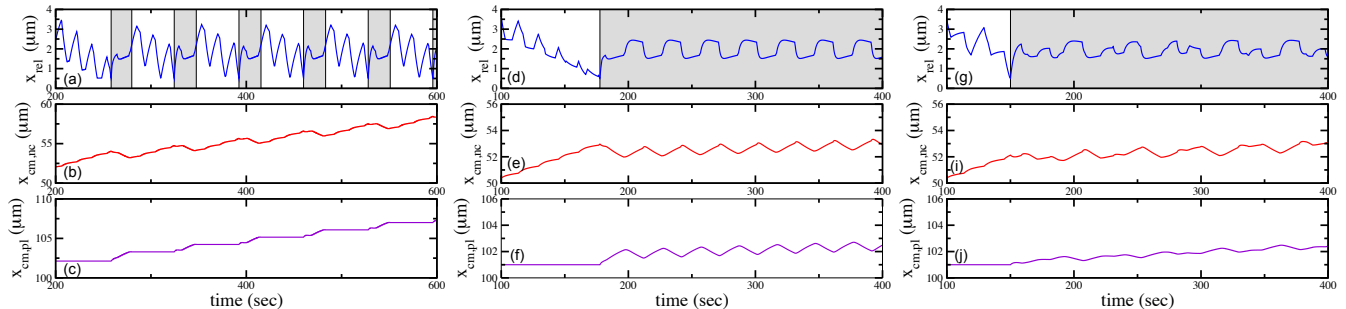


FIG. 2. (Color Online) (a)-(c) The relative distance between the two cells, the center of mass position of the neural crest, and the center of mass position of the placode cell, all as a function of time. Here,  $f_r = 0.01 nN$  and  $k = 5 nN/\mu m$ . The grey region in the top figure indicates when the interaction is tuned on. (d)-(f) The same as (a)-(c) but with  $f_r = 0.03 nN$  and  $k = 5 nN/\mu m$ . (g)-(i) Here,  $f_r = 0.03 nN$  and  $k = 5 nN/\mu m$  but with larger friction coefficients for the PLL cell.

fluctuations are due to activity and are not related to any temperature via a fluctuation-dissipation theorem. We will ultimately study the limit  $A_1 = A_2 = A_3 = A_4 = A$ . We have independent estimates for all but three parameters based either on experiments or prior modeling discussed in Ref. [15] or elsewhere. Specifically,  $k_1 = k_2 = 1 nN/\mu m$ ,  $x_{eq1} = 50 \mu m$ ,  $x_{eq2} = 5 \mu m$ ,  $l^\dagger = 48.5 \mu m$ ,  $l^\downarrow = 46.5 \mu m$ ,  $\gamma_{11} = 20 nNs/\mu m$ ,  $\gamma_{12} = 0 nNs/\mu m$ ,  $\gamma_{33} = 10 nNs/\mu m$ ,  $\gamma_{34} = 20 nNs/\mu m$ ,  $\gamma_2 = 20 nNs/\mu m$ , and  $\gamma_4 = 20 nNs/\mu m$ . For the interaction parameters, we know from single molecule experiments that  $f_c = 40 pN$  for N-cadherin and  $f_c = 70 pN$  for E-cadherin [30],  $k = k_f$  is of order  $1 nN/\mu m$  [31] (since  $k_c \approx k_f$ ), and  $N_0$  is of order 100 per pseudopod [32]. The only parameters we do not have independent estimates for are  $l_{eq}$ ,  $l_a$ , and  $A$ , though  $l_{eq}$  and  $l_a$  are determined by the appropriate lengthscales in the system. We set  $l_a = 0.5 \mu m$  and vary both  $l_{eq}$  and  $A$ .

To study this model, we implement 4th order Runge-Kutta integration scheme in the absence of noise. With noise, we implement a Euler-Marayuma integration scheme. We have checked our simulations against the analytical solution for some parameter values. For the single active dimer, there were two analytical solutions to be pieced together according to the cell's history. For the interacting active elastic dimer case there are eight analytical solutions to be pieced together according to each cell's history—two for each cell and two more cases for the interaction spring either on or off. Given the plurality of solutions, the majority of our results are based on simulations.

*Results:* To classify the types of interactions between the two different cells, we study the cell dynamics as a function of the junction spring stiffness,  $k$ , and the rupture force between cadherin molecules. We focus on  $x_{rel} = x_2(t) - x_3(t)$ ,  $x_{cm,pl}(t) = \frac{1}{2}(x_1(t) + x_2(t))$ , and  $x_{cm,nc}(t) = \frac{1}{2}(x_3(t) + x_4(t))$ . We initialize the NCL cell some distance away from the PLL cell and iterate until they interact. As a result of the asymmetry in the friction coefficients of the NCL cell, it will migrate towards the PLL cell, mimicking the movement of the NCL cell

toward the PLL cell due to chemotaxis, or a chemical gradient. The PLL cell, on the other hand, does not move (on its own) since there is no asymmetry in its friction coefficients. Figure 2(a)-(c) plots these quantities for  $f_r = 0.01 nN$  and  $k = 5 nN/\mu m$  as they interact. For these particular values, the cell springs are able to rupture the interaction spring, i.e. separate. But as the NCL cell, again, moves toward the PLL cell, the two cells interact again and the process repeats ad infinitum. We classify this dynamic state as *chase-and-run* behavior since the interaction spring is ruptured with the PLL cell pulling away from the NCL cell. Note that the position center of mass of the PLL cell only changes when in contact with the NCL cell.

Now we increase the rupture force to  $f_r$  to  $0.03 nN$ . See Fig. 2(d)-(f). At this increased rupture force for the cadherin molecules, the interaction spring always remains on, i.e. the two cells never separate once they interact. We dub this dynamic state as *clumping*. In the presence

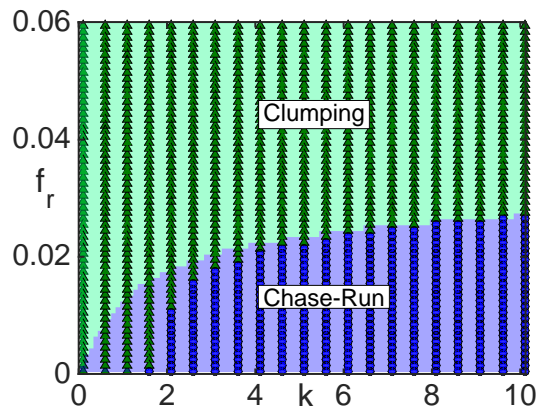


FIG. 3. (Color Online) Chase-Run and Clumping states for the two-cell model for the parameter values noted in the text. The symbols, blue circles (Chase-Run) and green triangles (Clumping) indicate simulation data, while the corresponding blue and green shaded regions correspond to the analytical result. The units of  $k$  are  $nN/\mu m$  and the units of  $f_r$  are  $nN$ .

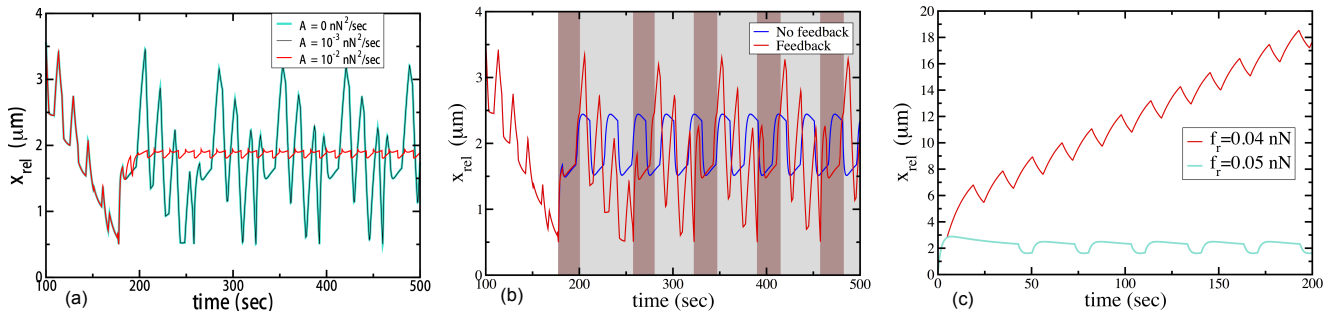


FIG. 4. (Color Online) (a) The relative distance between the cells with and without noise with variance  $A$  on each of the four beads (b) The relative distance between the two cells with and without feedback. The brown shading represents the presence of the interaction spring in the chase-and-run case, the clumping case. (c) Two cells moving apart from each other are not always able to rupture the interaction spring, i.e. escape. It depends on the rupture force.

of the chemotaxis and one sedentary cell, chase-and-run and clumping are the two behaviors one can observe in terms of how the cells come into contact. If we increase the two friction coefficients of the PLL cell such that the time scales are different for each cell, for  $f_r = 0.01 \text{ nN}$  and  $k = 5 \text{ nN}/\mu\text{m}$ , we observe quasiperiodic behavior in the relative distance between the cells. See Fig. 2(g)-(i).

To summarize our findings in terms of searching for chase-and-run and clumping dynamics as a function of the interaction spring stiffness and the rupture force, we present a phase diagram as a function of  $k$  and  $f_r$  in Fig. 3. The system transitions from chase-and-run at smaller rupture force to clumping at larger rupture forces. As the interaction spring stiffness increases far beyond the cell spring stiffness, the energetics is dominated by the interaction spring and the dependence on the rupture force on the transition decreases. We can estimate the transition line by looking at the case where each cell spring is in its contracting phase (smaller equilibrium spring length) so that each cell spring maximally pulls on the interaction spring to potentially rupture it.

We also investigate the model in the presence of active noise due to the presence of fluctuations in the myosin motors, for example. See Fig. 4(a). We find that the phase-diagram in Fig. 3 is robust to small fluctuations (see Fig. 4(a) for an example). However, a system undergoing chase-and-run dynamics in the absence of noise can be driven to clumping with large enough fluctuations. We have assumed here uncorrelated, or Gaussian noise, for simplicity. Should active noise be an important contribution, we anticipate fluctuations that correlate with motor activity, so that correlated noise may indeed be a more accurate representation of the biomechanics.

We now discuss the phase diagram in the context of the NC-PL experiments [3]. The authors of Ref. [3] conjectured that the switching of  $N$ - to  $E$ -cadherin binding drove the system from chase-and-run to clumping dynamics. We observe that here as well within the appropriate force scale. As mentioned earlier, the rupture force for  $N$ -cadherin is approximately  $40 \text{ pN}$ , while for  $E$ -cadherin, it is approximately  $70 \text{ pN}$ . We observe, for

example for  $k = 2$ , the doubling of rupture from  $10 \text{ pN}$  to  $20 \text{ pN}$  drives the system from chase-and-run to clumping. The experimentalists also conjectured that feedback between the cadherin and integrin is important for the chase-and-run dynamics – the more cadherin bind, the less integrin bind [3]. We, however, observe chase-and-run behavior even without any feedback between the two types of molecules. We can, of course, incorporate this feedback into our model as follows. If the interaction spring is on, the friction coefficients on both sides of the spring are decreased, say, by half (in both states for the NC cell). With this feedback, we observe that the chase-and-run state occupies a larger part of parameter space. For instance, with no feedback, the transition for  $k = 5 \text{ nN}/\mu\text{m}$  occurs at  $f_r = 0.021 \text{ nN}$  but with the feedback, the transition occurs at  $f_r = 0.023 \text{ nN}$ . Alternatively, a clumped system with no feedback can be driven to the chase-and-run state with feedback. See Fig. 4(b).

Finally, we address the issue of polarity. Polarity, here, is determined by the asymmetry in friction. If two cells initially moving toward each other, interact and then change polarity, the relative distance between them would decrease as they meet, and then increase as they interact and reverse direction. This behavior is known as contact-inhibition-locomotion (CIL) [33]. We conjecture that feedback between the cadherin and integrin binding could drive the cell to change its polarity and, therefore, potentially reverse direction. If the integrin binding becomes weaker one side of the cell due to molecules participating more in the cadherin junctions than in the focal adhesions, then integrin binding on the other side of the cell may increase to compensate. This increase in ultimately friction on the other side of the cell may be enough to begin to generate motion away from the “other” cell. If the two cells rupture the interaction spring between them, the two cells each go “their merry way”. Therefore rupture is an important part of the process. Within our model, it turns out that cells cannot always rupture the interaction spring between them, even if both cells are moving away from each other. See Fig. 4(c). This is counterintuitive at first but makes sense since the interac-

tion spring does not allow the cell springs to transition as readily between the two contracting and extending states so that each cell cannot escape each other.

*Discussion:* We have developed a one-dimensional mesoscopic model to describe the interaction between two cells mediated by N/E-cadherin. Like the experiments [3], we observe a transition from chase-and-run dynamics to clumping dynamics when switching from N- to E-cadherin. In the chase-and-run case, the NC cell acts as elastic herder controlling the motion of the PLL cell by interacting with it. This herding sheep analogy is distinct from the horse-carrot analogy presented in Ref. [3]. With our phase diagram, we can predict which behavior will occur depending on the rupture force of a single binding molecule that can be tested with genetic modification of both types of cadherins. We have also addressed the types of interactions two different motile cells can have in one-dimensional migration. Our model can be adapted to groups of NCL and PPL cells with each cell described as a group of active springs and there being interaction springs between each cell with the interaction springs between the NCL and PLL having a lower rupture threshold

than the interaction springs between two PLL cells.

Our model connects molecular and cellular scales to provide a mechanistic understanding of collective migration of heterogeneous cell populations that combine mesenchymal migratory properties and cadherin based cell-cell junctions. It may, therefore, not only apply to the enhanced migration of neural crest cells during morphogenesis, but also provide insights into the microscopic mechanical interactions between co-migrating cancer cells and non-tumorigenic cells, which are known to have significantly different mechanical and adhesion properties [34]. Finally, our results demonstrate that a quantitative framework of cell-cell interaction should include molecular rupture forces [29] as well as the mechanosensitive activity of the cytoskeletal machinery to help inform the case of more than two interacting cells with varying degrees of cell motility, thereby quantifying the coordinated migration of cells.

DM and JMS acknowledge support from DMR-CMMT-1507938. NB and MD were partially supported by a Cottrell College Science Award from Research Corporation for Science Advancement.

- 
- [1] P. Friedl, Y. Hegerfeldt, M. Tusch, "Collective cell migration in morphogenesis and cancer", *Int. J. Dev. Biol.* **48**, 441 (2004).
- [2] C. Gaggioli, *et al.*, "Fibroblast-led collective invasion of carcinoma cells with differing roles for RhoGTPases in leading and following cells", *Nat. Cell Biol.* **9**, 1392 (2007).
- [3] E. Theveneau, *et al.*, "Chase-and-run between adjacent cell populations promotes directional collective migration", *Nat. Cell Biol.* **15**, 763 (2013).
- [4] E. Theveneau and R. Mayor, "Neural crest delamination and migration: From epithelium-to-mesenchyme transition to collective cell migration", *Dev. Biol.* **366**, 34 (2012).
- [5] G. Schlosser, "Making senses development of vertebrate cranial placodes", *Int. Rev. Cell Mol. Biol.* **283**, 129 (2010).
- [6] A. Mogilner, "Mathematics of cell motility: have we got its number?", *J. Math. Biol.* **58**, 105 (2009).
- [7] K. Keren, Z. Pincus, G. M. Allen, E. L. Barnhart, G. Marriott, A. Mogilner, and J. A. Theriot, Mechanism of shape determination in motile cells, *Nature* **453**, 475 (2008).
- [8] K. V. Kumar, S. Ramaswamy, and M. Rao, "Active elastic dimers : Self-propulsion and current reversals on a featureless track", *Phys. Rev. E* **77**, 020102 (R) (2008).
- [9] E. L. Barnhart, G. M. Allen, F. Julicher, and J. A. Theriot, Bipedal Locomotion in Crawling Cells, *Biophys. J.* **98**, 933 (2010).
- [10] A. J. Loosely and J. X. Tang, Stick-slip motion and elastic coupling in crawling cells, *Phys. Rev. E* **86**, 031908 (2012).
- [11] E. Tjhung, A. Tiribocchi, D. Marenduzzo, M. Cates, "A minimal physical model captures the shapes of crawling cells", *Nat. Comm.* **6**, 5420 (2015).
- [12] B. Camley, *et. al.*, "Polarity mechanisms such as contact inhibition of locomotion regulate persistent rotational motion of mammalian cells on micropatterns", *Proc. Natl. Acad. Sci. USA* **111**, 14770 (2014).
- [13] F.J. Segerer, F. Thuroff, A. Piera Alberola, E. Frey, J.O. Radler, "Emergence and Persistence of Collective Cell Migration on Small Circular Micropatterns" *Phys. Rev. Lett.* **114**, 228102 (2015).
- [14] B. Li and Sean X. Sun, "Coherent motions in confluent cell monolayer sheets", *Biophys. J.* **107**, 1532 (2014).
- [15] J. H. Lopez, Moumita Das, and J. M. Schwarz, "Active elastic dimers: Cells crawling on a rigid track", *Phys. Rev. E* **90**, 032707 (2014).
- [16] M. Abercrombie and J. E. Heaysman, "Observations on the social behaviour of cells in tissue culture. I. Speed of movement of chick heart fibroblasts in relation to their mutual contacts", *Exp. Cell Res.* **5**, 111131 (1953).
- [17] C. Carmona-Fontaine, *et al.*, "Contact inhibition of locomotion in vivo controls neural crest directional migration", *Nature* **18**, 456 (2008).
- [18] P. Friedl, K. S. Zanker, and E. B. Brocker, Cell migration strategies in 3-D extracellular matrix: Differences in morphology, cell matrix interactions, and integrin function, *Micro. Res. Tech.* **43**, 369 (1998).
- [19] A.D. Doyle, R.J. Petrie, M. Kutys, L. Matthew, and K. M. Yamada, "Dimensions in cell migration", *Curr. Opin. Cell Biol.* **25**, 642 (2013).
- [20] A. Pathak and S. Kumar, "Transforming potential and matrix stiffness co-regulate confinement sensitivity of tumor cell migration", *Integr. Biol.* **5**, 1067 (2013).
- [21] M. Mak, C. A. Reinhart-King, and D. Erickson, "Micro-fabricated Physical Spatial Gradients for Investigating Cell Migration and Invasion Dynamics", *PLoS ONE* **6**: e20825 (2011).
- [22] S. I. Fraley, Y. Feng, A. Giri, G. D. Longmore, D.

- Wirtz, Dimensional and temporal controls of three-dimensional cell migration by zyxin and binding partners, *Nat. Comm.* **3**, 719 (2012).
- [23] S. Tojkander, G. Gateva, P. Lappalainen, Actin stress fibers: Assembly, dynamics and biological roles, *J. Cell Sci.* **125**, 1 (2012).
- [24] B. Guo and W. H. Guilford, “Mechanics of actomyosin bonds in different nucleotide states are tuned to muscle contraction”, *Proc. Natl. Acad. Sci. USA* **103**, 9844 (2006).
- [25] P. Kanchanawong, G. Shtengel, A. M. Pasapera, E. B. Ramko, M. W. Davidson, H. F. Hess, and C. M. Waterman, “Nanoscale architecture of integrin-based cell adhesions”, *Nature* **468**, 580 (2010).
- [26] F. Kong, A. J. Garcia, A. P. Mould, M. J. Humphries, and C. Zhu, “Demonstration of catch bonds between an integrin and its ligand”, *J Cell Biol.* **185**, 1275 (2009).
- [27] M. Dembo and Y.-L. Wang, Stresses at the cell-to-substrate interface during locomotion of fibroblasts, *Biophys. J.* **76**, 2307 (1999).
- [28] B. D. Hoffman and A. S. Yap, “Towards a dynamic understanding of cadherin-based mechanobiology” *Trends Cell Biol.* **25**, 803 (2015).
- [29] U. Seifert, Rupture of Multiple Parallel Molecular Bonds under Dynamic Loading, *Phys. Rev. Lett.* **84**, 2750 (2000).
- [30] P. Panorchan, *et al.* “Single-molecule analysis of cadherin-mediated cell-cell adhesion”, *J. Cell Sci.* **119**, 66 (2006).
- [31] T. Bornschlogl, *et al.*, “Filopodial retraction force is generated by cortical actin dynamics and controlled by reversible tethering at the tip”, *Proc. Natl. Acad. Sci. USA* **110**, 18928 (2013).
- [32] B.-A. T. Quang, M. Mani, O. Markova, T. Lecuit, and P.-F. Lenne, “Principles of e-cadherin supramolecular organization *in vivo*”, *Curr. Biol.* **23**, 2197 (2013).
- [33] A. Roycroft and R. Mayor, “Molecular basis of contact inhibition of locomotion”, *Cell Mol. Life Sci.* **73**, 1119 (2016).
- [34] W. Song, C.K. Tung Y.C. Lu, Y. Pardo, M. Wu, M. Das, D. Kao, S. Chen, and M. Ma, “Dynamic self-organization of microwell-aggregated cellular mixtures”, *Soft Matter* **12**, 5739 (2016).